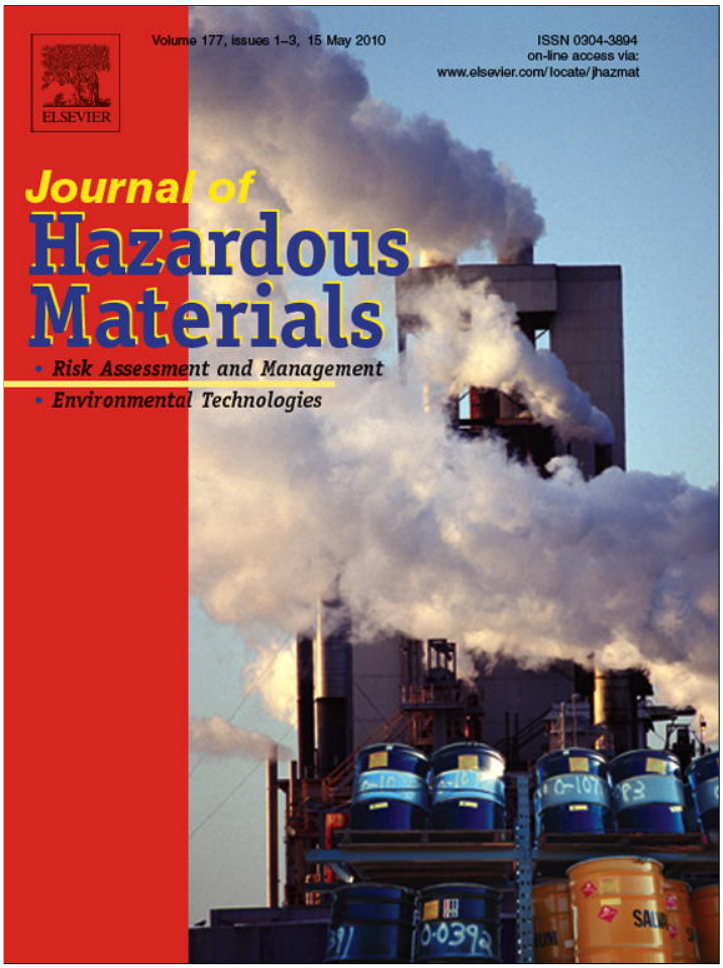

Journal of Hazardous Materials 177 (2010) 864–875

Contents lists available at ScienceDirect

Journal of Hazardous Materials

journal homepage: www.elsevier.com/locate/jhazmat

Fabrication of porous TiO_2 film on Ti foil by hydrothermal process and its photocatalytic efficiency and mechanisms with ethyl violet dye

Fu-Der Mai [b], Wen-Lian William Lee [c], Jia-Lin Chang [a], Shou-Ching Liu [a], Chia-Wei Wu [a], Chiing-Chang Chen [a,*]

[a] Department of Science Application and Dissemination, National Taichung University, No. 140, Min-Shen Road, Taichung 403, Taiwan, ROC
[b] Department of Biochemistry, School of Medicine, Taipei Medical University, Taipei 110, Taiwan, ROC
[c] Department of Occupational Safety and Health, Chung-Shan Medical University, Taichung 402, Taiwan, ROC

ARTICLE INFO

Article history:
Received 1 August 2009
Received in revised form 31 October 2009
Accepted 24 December 2009
Available online 7 January 2010

Keywords:
Porous TiO_2 film/Ti foil
Photocatalytic
Ethyl violet
Hydrothermal process

ABSTRACT

Most of commercial dyes and pigments have rather complicated polyaromatic chemical structures with prolonged lifetime surviving in the Mother Nature. However, TiO_2 has been reported as one of the best photocatalytic candidates for degrading dye pollutants. In this report, TiO_2 film/Ti foil was prepared by hydrothermal reaction in alkali solution, the porous TiO_2 film with microcrystalline structure has been obtained. The porous structure of TiO_2 film was analyzed and characterized by XRD, FE-SEM and XPS. This is the first report that demonstrates that TiO_2 film/Ti foil has an excellent commercial application potential for photocatalytic degradation of Ethyl Violet (EV). Especially, because of refluxing at 100 °C, the porous TiO_2 film structure remained undisturbed, and EV decomposed in the period of 20 h. In addition, porous TiO_2-mediated EV photo degradation mechanism has been proposed, as intermediates are isolated and clearly identified by GC-MS and HPLC-PDA-ESI-MS.

1. Introduction

Over 700,000 tons dyes and pigments are produced worldwide, of which about 20% are in industrial effluents from textile dyeing and finishing processes annually [1]. Most of these dyestuffs have complicated polyaromatic structures, and they cannot be treated successfully by conventional degradation methods [2]. However, the TiO_2-mediated photocatalysis processes have been demonstrated successfully to degrade dye pollutants [3–9]. It was noted especially that the triphenylmethane dyes, containing *N*-alkylamine groups appeared to be photodegradable [10–13]. As triphenylmethane dyes are used extensively in the textile industry as well as the paper, food, cosmetic, and leather industries [1,2]. For example, thyroid peroxidase-catalyzed oxidation of the triphenylmethane dyes results in the formation of various *N*-dealkylated primary and secondary aromatic amines, which have structures similar to aromatic amine carcinogens [14]. Photocatalytic degradation of nitrogen-containing aromatics has also shown that either photogenerated electrons or hydroxyl radicals act concurrently to transform the nitrogen-containing groups [15,16].

Titanium dioxide (TiO_2) is a photocatalytic material with applications in fields such as environmental purification [3–9], decomposition of carbonic acid gases, and solar cells [17–22]. Several techniques can be used to prepare TiO_2 thin films, including thermal oxidation of titanium, anodic oxidation, and sputtering [23–32]. Especially, TiO_2 films have attracted much attention on wetting behavior [33], oxygen adsorption [34], and heterogeneous photo-catalysis [29]. One of the most active research areas has been environmental remediation, including self-cleaning materials. Indeed, many organic pollutants can be degraded and ultimately mineralized using TiO_2 photo-catalysts in the presence of UV or visible light irradiation [17,19,21]. For example, TiO_2-based photo-catalysts have been used to break down organic compounds in wastewater [11–13,29]. One of the most interesting investigations was the degradation of organic solutions using TiO_2 nanotube layers [20,29]. The nanotube layers provide a large specific surface area, to produce a greater photocatalytic activity. However, porous TiO_2 films have never been prepared and studied sufficiently in the TiO_2-assisted photodegradation system.

In this current study, the porous TiO_2 films/Ti foils have been first prepared successfully. Grown in alkali solution at different reflux times, a porous TiO_2 film with high surface area to volume ratios has been obtained on the Ti foils surface. In order to get the crystalline porous TiO_2 film, structural evolution versus reflux time was performed and monitored by FE-SEM and XRD. In addition, the photocatalytic activity of porous TiO_2 films has been demonstrated to provide the total degradation of EV dye. Using GC-MS and HPLC-

* Corresponding author. Tel.: +886 4 2218 3406; fax: +886 4 2218 3530.
E-mail addresses: ccchen@mail.ntcu.edu.tw, ccchen@ms3.ntcu.edu.tw (C.-C. Chen).

0304-3894/$ – see front matter © 2010 Elsevier B.V. All rights reserved.
doi:10.1016/j.jhazmat.2009.12.113

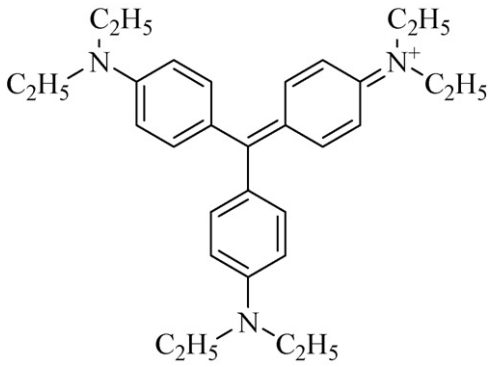

Fig. 1. Chemical structure of EV.

PDA-ESI-MS, most of the reaction intermediates have been isolated and characterized. Finally, under the porous TiO_2 film/UV process, the mechanism of EV dye photodegradation has been proposed.

2. Experimental section

2.1. Materials and reagents

TiO_2 foil (99.9% purity, 150 mm × 150 mm × 0.25 mm) was purchased from Sigma. TiO_2 powder (Degussa P25), a mixture of anatase and rutile (8:2), was used as received as a standard without further purification. EV (ethyl violet; basic violet 4; *N,N,N′,N′,N″,N″*-hexaethylpararosaniline; $C_{31}H_{42}N_3Cl$) and 4-(*N,N*-diethylamino)-4′-(*N′,N′*-diethylamino)benzophenone (DDBP) were obtained from Tokyo Kasei Kogyo Co. The chemical structure of EV is shown in Fig. 1. 4-Aminophenol (AP; analytical standard) was purchased from Riedel-de Haen. Reagent-grade ammonium acetate, nitric acid, sodium hydroxide, hydrogen chloride, and HPLC-grade methanol and acetone were purchased from Merck.

2.2. Fabrication of porous TiO_2 film by reflux

Ti foils were ultrasonically washed in HPLC-grade acetone three times before use. To prepare TiO_2 film, a piece of Ti foil (75 mm × 75 mm × 0.25 mm) and 3 L, 10 M NaOH aqueous solution was conducted as shown in the scheme as shown in Fig. 2. After refluxing reflux 12, 24, 48 h, r12-TiO_2, r24-TiO_2, r48-TiO_2, respectively. TiO_2/Ti foil was further neutralized with 0.1 M HCl aqueous solution, washed with de-ionized water/ethanol several times, and dried under nitrogen gas.

2.3. Photocatalytic experiments

The schematic of diagram of experimental apparatus was shown in reference [35]. The C-75 Chromato-Vue Cabinet of UVP provides a wide area of illumination from the 15-W 365 nm tubes positioned on two sides of the cabinet interior. A mixture solution was prepared by adding porous TiO_2 film to a 250 mL aqueous containing the EV at appropriate concentrations. The pH value of the solution was adjusted by adding of either NaOH or HNO_3 solution. Prior to irradiation, the mixture solution was magnetically stirred in the dark for ca. 30 min to ensure the establishment of adsorption–desorption equilibrium. Irradiations were carried out using two lamps (UV-365 nm, 15 W). At given irradiation time intervals, the solution was sampled (5 mL), centrifuged, and subsequently filtered through a Millipore filter (pore size, 0.45 μm) to separate the particles. Blank experiments in a beaker without addition of porous TiO_2 film showed slight decolorization of the

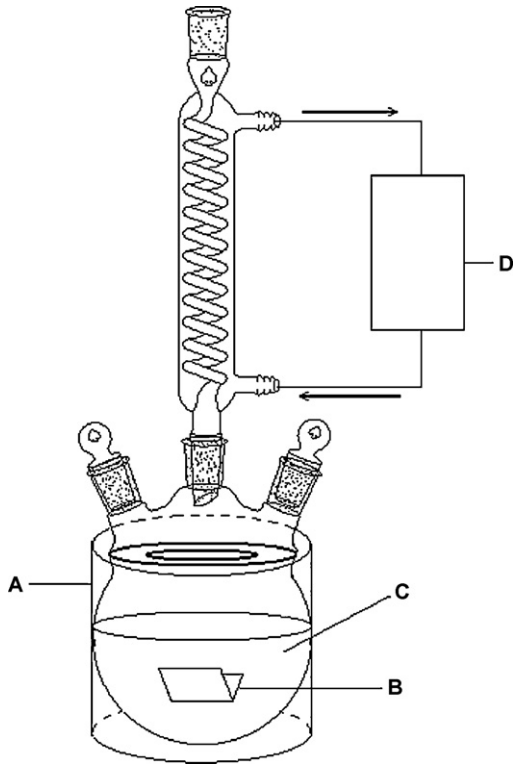

Fig. 2. Reflux apparatus: (A) heating mantle; (B) Ti foil; (C) 3 L glasses reactor include 1 L 10 M NaOH; (D) refrigerator circulating water bath.

irradiated solution and confirmed the expected stability of EV dye under UV light irradiation. Addition of porous TiO_2 film to solutions containing 10 mg L^{-1} of EV did not alter the stability of the dye in the dark.

2.4. Instruments and analytical methods

The surface morphologies of the films were examined by scanning electron microscopy (FE-SEM, JSM-7401F, JEOL) and the crystal structures were investigated by X-ray diffractometer analysis (XRD, MXP18, MAC Science). The chemical composition of the thin films was investigated by X-ray photoelectron spectroscopy (XPS, PHI Quantera SXM, ULVAC-PHI XPS). XPS spectra were collected by exciting the film without pre-treatment with an Al Kα X-ray source. The Al Kα radiation was generated with a voltage of 15 kV. The spectrometer was calibrated using the Ag 3d5/2 core line. The binding energy values reported in the present work were corrected by using the C1s peak at 284.8 eV for taking charging effects into account.

A Waters ZQ LC/MS system – equipped with a Waters 1525 Binary HPLC pump, a Waters 2996 Photodiode Array Detector, a Waters 717plus Auto sampler, and a Waters micromass-ZQ4000 Detector – was used. The degradation was monitored by measuring the absorbance with a Photodiode Array Detector (PDA). After each irradiation cycle, the amount of the residual dye was determined by HPLC-PDA. The analysis of organic intermediates was accomplished by HPLC-PDA-ESI-MS after the readjustment of the chromatographic conditions in order to make the mobile phase compatible with the working conditions of the mass spectrometer. Two different kinds of eluent were employed in this study. Solvent A was 25 mM aqueous ammonium acetate buffer (pH 6.9) while solvent B was methanol. LC was carried out on an Atlantis™ dC18 column (250 mm × 4.6 mm i.d., dp = 5 μm). The flow rate of the mobile phase was set at 1.0 mL min^{-1}. A linear gradient was set as follows: t = 0 min, A = 95, B = 5; t = 20 min, A = 50, B = 50; t = 40–45 min, A = 10,

Table 1
Energy dispersive spectroscopy (EDS) of the porous TiO_2 film by reflux at different times.

Samples	EDS	
	Weight%	Atomic%
r12-TiO_2 (Ti-reflux, 12 h)	Ti (77.48%) O (12.89%) C (9.63%)	Ti (55.58%) O (27.67%) C (16.75%)
r24-TiO_2 (Ti-reflux, 24 h)	Ti (76.59%) O (16.47%) C (6.94%)	Ti (50.51%) O (32.52%) C (16.93%)
r48-TiO_2 (Ti-reflux, 48 h)	Ti (84.88%) O (12.51%) C (2.61%)	Ti (67.66%) O (29.85%) C (2.49%)

$B = 90$; $t = 48$ min, $A = 95$, $B = 5$. The column effluent was introduced into the ESI source of the mass spectrometer.

Solid-phase extraction (SPE) was employed for preconcentration of irradiated samples prior to GC-MS analysis. Oasis HLB (hydrophilic/lipophilic balance) was used as the sorbent, and this ensures good recovery of compounds in a wide range of polarities. The cartridges were placed in a vacuum cube (provided by Supelco) and conditioned with 5 mL of methanol and 5 mL of deionized water. After the conditioning step, 1000 mL aliquots of the irradiated samples were loaded at a flow rate of approximately 10 mL/min. Elution was performed with 5 mL of methanol. The eluates obtained were concentrated by solvent evaporation with a gentle nitrogen stream and recomposed to a final volume of 1 mL in methanol. The extracts were stored in amber vials and refrigerated until chromatographic analysis to prevent further degradation.

GC/MS analyses were run on a PerkinElmer AutoSystem-XL gas chromatograph interfaced to a TurboMass selective mass detector. Separation was carried out in a DB-5 capillary column (5% diphenyl/95% dimethyl-siloxane), 60 m, 0.25-mm i.d., and 1.0-μm thick film. A split–splitless injector was used under the following conditions: injection volume 1 μL, injector temperature 280 °C, split flow 10 mL/min. The helium carrier gas flow was 1 mL/min. The oven temperature program was 4.0 min at 40 °C, 4 °C/min to 80 °C (2 min), 8 °C/min to 280 °C (9 min). The autotuning software optimized typical MSD operating conditions. Electron impact (EI) mass spectra were monitored from 35 to 300 m/z. The ion source and inlet line temperatures were set at 220 and 280 °C, respectively.

3. Results and discussion

3.1. Characterization of material

3.1.1. FE-SEM-EDS

Fig. 3 shows SEM images of the porous TiO_2 films obtained by alkali aqueous reflux with Ti foil. Porous TiO_2 films have grown on top of the Ti foil with an oxide barrier layer separating the porous TiO_2 film from the titanium foil. From the top down image view, the porous surface is approximately 300–600 nm in diameter. The diameter of the surface was found to increase with the increase in reflux time. In addition, Fig. 3 (inset) shows an oblique view of the porous TiO_2 film at different reflux times. The film thickness determined by accounting for foreshortening from this image was found to be approximately 3.176, 3.012, and 2.680 μm corresponding to reflux of 12, 24, and 48 h respectively. The composition of the porous TiO_2 film was analyzed by an energy dispersive spectroscopy (EDS) study (Table 1) revealing the presence of Ti and O as the only elementary components with oxygen deficiency (Ti:O ~ 2:1 atomic ratio) in all the samples.

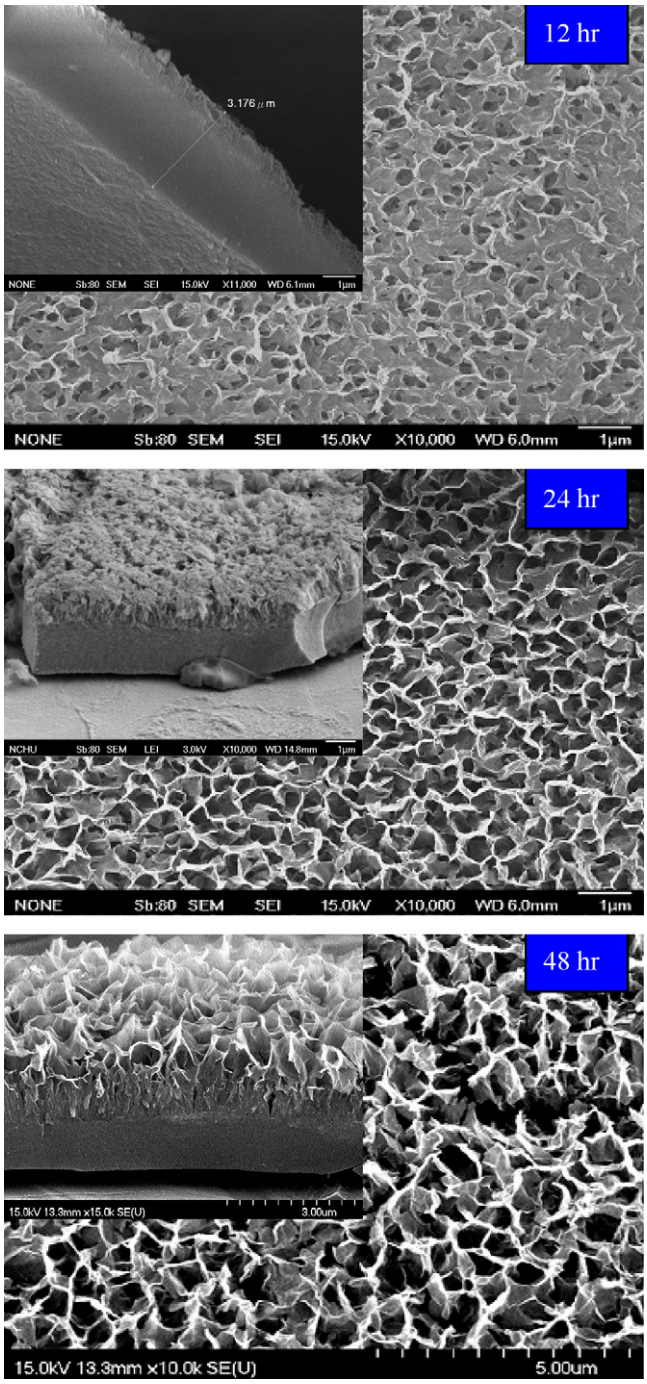

Fig. 3. FE-SEM of the as-prepared TiO_2 films. Reflux (a) 12 h, the oblique view showing thickness of film about 3.176 μm; (b) 24 h, the oblique view showing thickness of film about 3.012 μm; (C) 48 h, the oblique view about 2.680 μm.

3.1.2. XRD

Fig. 4 shows the XRD pattern of sample, which was prepared in 3 L, 10 M NaOH at 100 °C for 12, 24, 48 h. All the reflections can be readily indexed to P25-TiO_2 phase (JCPDS card no. 36-1451) except for those marked from the Ti foil. No obvious characteristic peaks are observed for other impurities. The characteristic line of anatase (1 1 2), (2 2 0) and rutile lines (2 0 2) appears on different reflux times while the anatase (0 0 2) only appears at the r12-TiO_2 film and r24-TiO_2 film. The intensity of the lines of rutile (0 0 2), (2 0 2) and anatase (1 1 2), (2 2 0) was observed to increase and then decrease with the increase in the reflux time.

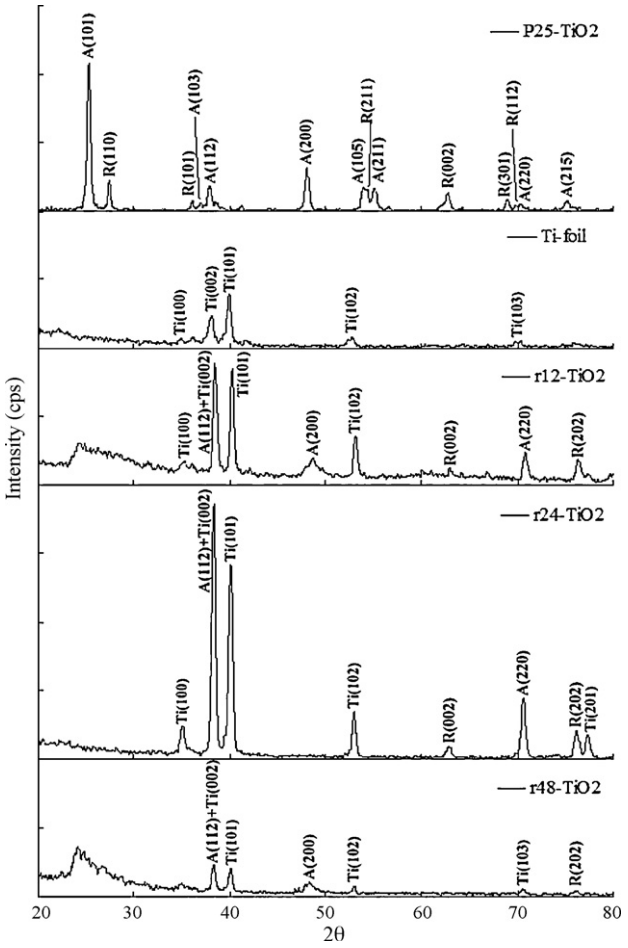

Fig. 4. XRD patterns of TiO_2 films obtained on Ti foil. Spectra from top to bottom correspond to P25-TiO_2, Ti foil, reflux time of 12, 24, 48 h (Ti foil prepared in 3 L 10 M NaOH solution, at 100 °C), respectively. (A: anatase phase, R: rutile phase).

3.1.3. XPS

Fig. 5 shows Ti2p XPS spectra of the Ti foil before and after the alkali reflux treatment at different times. In Fig. 5a, the binding energies of $Ti2p_{3/2}$ in P25-TiO_2, Ti-foil, r12-TiO_2, r24-TiO_2, and r48-TiO_2 are 457.8, 452.9, 458.2, 457.8, and 458.0 eV, respectively. In Fig. 5b, the binding energies of O1s in P25-TiO_2, Ti-foil, r12-TiO_2, r24-TiO_2, and r48-TiO_2 are 529.1, 529.7, 529.7, 529.4, and 529.2 eV, respectively. On porous films, a $Ti2p_{3/2}$ peak around 457.8 eV appeared similar with P25-TiO_2 of the peak.

3.2. Photocatalytic degradation of EV by porous TiO_2 film

3.2.1. Effect of reflux time

In photocatalytic processes, the amount of photocatalyst on Ti foil is an important parameter that can affect the degradation rate of organic compounds. The optimal catalyst films depend on the nature of the films [36]. Hence, the effect of photocatalyst films on Ti foil on the photodegradation rates of the EV dye was investigated by employing different reflux times of Ti foil varying from 12 to 48 h by 10 M alkali aqueous solution. As expected, the photodegradation rate of the EV was found to increase then decrease with the increase in the catalyst concentration (Fig. 6). The photolysis reaction and adsorption resulted a decrease about 4.5% and 7.7% in the EV concentration after 20 h while in the photocatalytic reaction the EV was completely decomposed after 20 h. Above 24 h reflux time, the initial rate of EV degradation was not affected further by a progressive increase. The maximal initial degradation rate for EV appears at 24 h reflux time. At room temperature, the oxidation of titanium metal by dissolved oxygen in water is very slow due to the limited surface oxidation layer. However, in the presence of alkali solution, the oxidation reaction can be accelerated drastically, and to form porous TiO_2 films on the surface of the Ti foil. The reaction between Ti and O_2 in an alkaline solution is generally recognized to produce TiO_2 (Eqs. (1) and (2)). Fig. 6 does show the trend as the TiO_2 formation once the reflux time increases. However, the TiO_2 formation rate fell gradually, this might be explained as the OH^- can be consumed by $Ti(OH)_4$, and then generate $Ti(OH)_6{}^{2-}$ as shown in Eq. (3).

$$Ti + O_2 + 2H_2O \rightarrow Ti(OH)_4 \quad (1)$$

$$Ti(OH)_4 \rightarrow TiO_2 + 2H_2O \quad (2)$$

$$Ti(OH)_4 + 2OH^- \rightarrow Ti(OH)_6{}^{2-} \quad (3)$$

In the following experiment, we chose r24-TiO_2 as the optimum film.

3.2.2. Effect of pH

The surface of TiO_2 would charge negatively and adsorb cationic species easily under pH > pHzpc (zero point charge) conditions. Under the reverse conditions, it would adsorb anionic ones [37]. However, the adsorption of the substrate onto the TiO_2 surface directly affects the occurrence of electron transfer between the excited dye and TiO_2 and further influences the degradation rate. The surface becomes positively charged, and the number of adsorption sites may decrease above the isoelectric point of TiO_2. The photodegradation rate of the EV dye as a function of reaction pH is shown in Fig. 7. The photodegradation rate of the EV dye was found to decrease then increase with increases in pH value. A higher degradation rate under an acid pH is seen also for the degradation of azo dyes in TiO_2-mediated experiments due to the efficient electron-transfer process that occurs with surface complex bond formation [38,39]. Hydroxyl radicals can be formed by the reaction between hydroxide ions and positive holes. The positive holes are considered major oxidation species at low pH while hydroxyl radicals are the predominant species at neutral or high pH levels [40]. An additional explanation for the pH effects is related to changes in the specification of the dye. That is, protonation or deprotonation of the dye can change its adsorption characteristics and redox activity [41]. Under neutral pH values, this surface is not easily charged and the photodegradation of EV became therefore slower. With higher pH values, the formation of active $^{\bullet}OH$ species is favored, due not only to improved transfer of holes to the adsorbed hydroxyls, but also to electrostatic abstractive effects between the negatively charged TiO_2 film and the operating cationic dyes. Hence, the photodegradation of EV was the fastest. Our results indicate that the TiO_2 surface is negatively charged, and the EV adsorbs onto the TiO_2 surface through the positive ammonium groups. The proposed adsorption mechanisms are in good agreement with earlier reports [42]. Although the EV dye can adsorb onto the TiO_2 surface to some extent in alkaline media, when the pH value is too high (pH 9), the dye molecules will change into a colorless carbinol base [9,43].

3.2.3. Effect of dye concentration

By varying the initial dye concentration from 0.01 to 0.05 g L^{-1} with r24-TiO_2 film as catalyst (pH 9), its effect on the degradation rate could be determined. Degradation efficiency is inversely affected by the dye concentration. This negative effect can be explained as follows; as the dye concentration is increased, the equilibrium adsorption of dye on the catalyst surface active sites increases; hence competitive adsorption of OH^- on the same sites decreases, meaning a lower formation rate of $^{\bullet}OH$ radical, which is the principal oxidant necessary for a high degradation efficiency. On the other hand, considering the Beer–Lambert law, as the initial dye

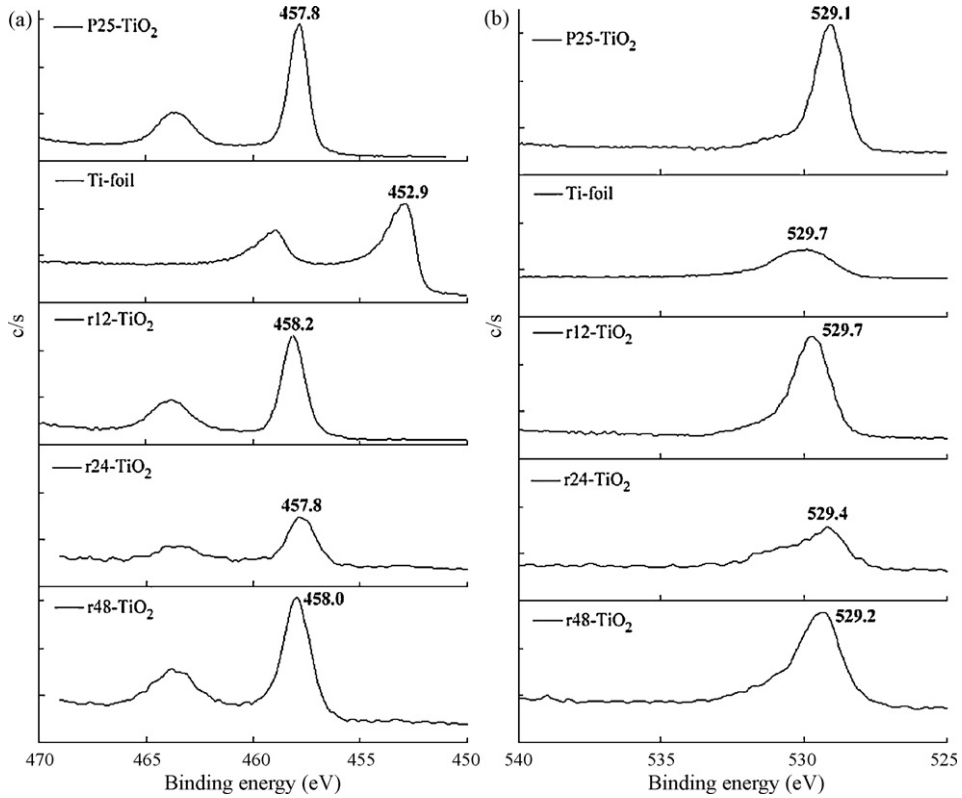

Fig. 5. (a) Ti $2p_{3/2}$ and (b) O1s XPS spectra of the porous TiO_2 films by different reflux times.

concentration increases, the path length of photons entering the solution decreases, resulting in lower photon adsorption on catalyst particles and, consequently, a lower photodegradation rate.

3.2.4. Comparison of TiO_2 and reused-TiO_2 degradation efficiencies

Initially, the experiments were performed under UV irradiation with r24-TiO_2 film as catalyst, and the photodegradation efficiency was observed. To compare the efficiency, reused-TiO_2 catalyst was tried under the same process conditions. Typical results are shown in Fig. 8. They show that reused r24-TiO_2 catalyst exhibits lower photocatalytic activity than the r24-TiO_2 film as catalyst, and the explanation is that as the surface active sites of reused-TiO_2 catalyst decrease, the equilibrium adsorption of dye and adsorption of OH^- on the catalyst surface active sites also decrease, which means a lower degradation efficiency. These results agree with those obtained concerning the photocatalytic degradation of dye [44,45]. A similar photocatalytic degradation of malachite green has been reported [46].

3.3. Separation of the intermediates

Temporal variations occurring in the solution of EV dye during the degradation process with UV irradiation were examined using HPLC coupled with a photodiode array detector and ESI mass spectrometry. The chromatograms at pH 5 are illustrated in Fig. 9, recorded at 580, 350, and 300 nm. With irradiation up to 36 h at pH 5, 21 components were identified, all with retention time of less than 50 min. We denoted the EV dye and its related intermediates as species A–J, a–f, a′–b′, and α–γ. Except for the initial EV dye (peak A), the other peaks initially increased before sub-

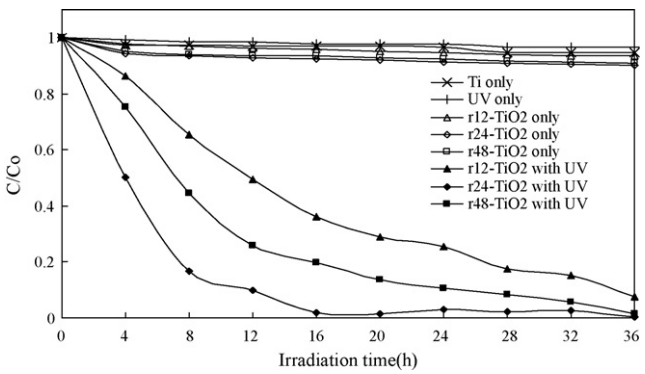

Fig. 6. Influence of reflux time was examined by the degradation rate for the decomposition of EV at pH 5. The value of C/Co was expanded on the right. Experimental conditions: dye concentration (10 mg L^{-1}), absorbance was followed at 580 nm, continuous stirring, and irradiation time 36 h.

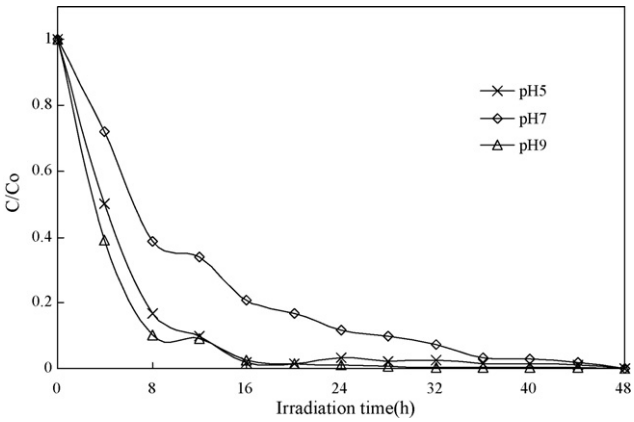

Fig. 7. The pH effect on the EV degradation rate: r24-TiO_2 film as catalyst; EV, 10 mg L^{-1}.

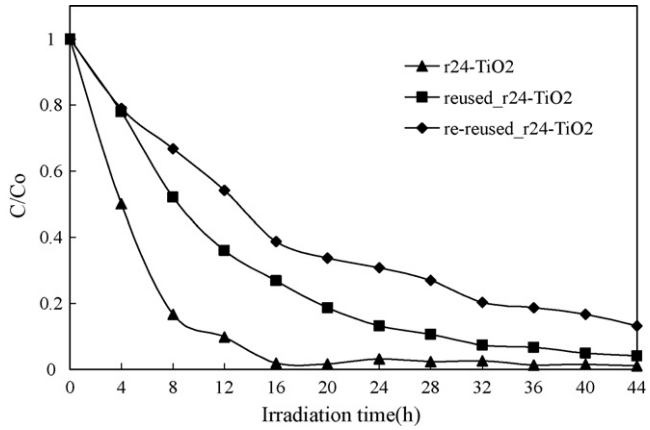

Fig. 8. Comparison of degradation rate for the decomposition of EV under r24-TiO_2 film with being reused. Conditions: r24-TiO_2 film as catalyst; EV, 10 mg L^{-1}; pH 5.

sequently decreasing, indicating formation and transformation of the intermediates. Fig. 1S of supporting information shows the GC chromatogram obtained for a SPE extract of EV solution after 44 h of irradiation. Up to six compounds could be detected as possible degradation intermediates. We denoted these intermediates as compounds I–VI.

3.4. Identification of the intermediates

3.4.1. UV–vis spectra of the intermediates

The maximum absorption of each intermediate in the visible and ultraviolet spectral region is depicted in Table 2. They are identified as A–I, a–f, a′–d′, and α–γ corresponding to the peaks A–I, a–f, a′–d′, and α–γ in Fig. 9, respectively. The absorption maximum of the spectral bands shifts from 590.5 nm (spectrum A) to 555.4 nm (spectrum J), 371.6 nm (spectrum a) to 340.6 nm (spectrum f), 370.4 nm (spectrum a′) to 367.9 nm (spectrum b′), and 302.4 nm (spectrum α) to 288.1 nm (spectrum γ). These shifts of the absorption band are presumed to result from the formation of a series of *N*-de-ethylated or *N*-hydroxyethylated intermediates. From these results, several groups of intermediates can be distinguished.

The first group is marked in the chromatogram and illustrated in Fig. 9a. The intermediates of *N*-de-ethylated EV dye have the wavelength position of its major absorption band moved toward the blue region, λ_{max}, A (EV), 590.5 nm; B, 585.6 nm; C, 577.1 nm; D, 572.2 nm; E, 583.2 nm; F, 574.6 nm; G, 566.3 nm; H, 574.9 nm; I, 560.2 nm; J, 555.4 nm. The *N*-de-ethylation of the EV dye caused the wavelength shifts depicted in Table 2 because of attack by one of the active oxygen species on the *N*,*N*-diethyl or *N*-ethyl group. Examination of Table 2 suggests that EV dye is *N*-de-ethylated in a stepwise manner (i.e., ethyl groups are removed one by one as confirmed by the gradual peak wavelength shifts toward the blue region), which has been reported [43].

The second and third groups are marked in the chromatogram and illustrated in Fig. 9b. Destruction of EV yields DAP, DDBP, and their *N*-de-ethylated products *N*-hydroxyethylated intermediate. The *N*-de-ethylation of the DDBP and the *N*-hydroxyethylated intermediates of the *N*-de-ethylated DDBP species, produced by cleavage of the EV chromophore ring structure, have the wavelength position of its major absorption band moved toward the blue region, λ_{max}, a, 371.6 nm; b, 366.7 nm; c, 362.1 nm; d, 367.9 nm; e, 357.2 nm; f, 340.6 nm and a′, 370.4 nm; b′, 367.9 nm. The proposed intermediate (a) has been compared with standard material of 4-(*N*,*N*-diethylamino)-4′-(*N*′,*N*′-diethylamino)benzophenone. The retention time and absorption spectra are identical.

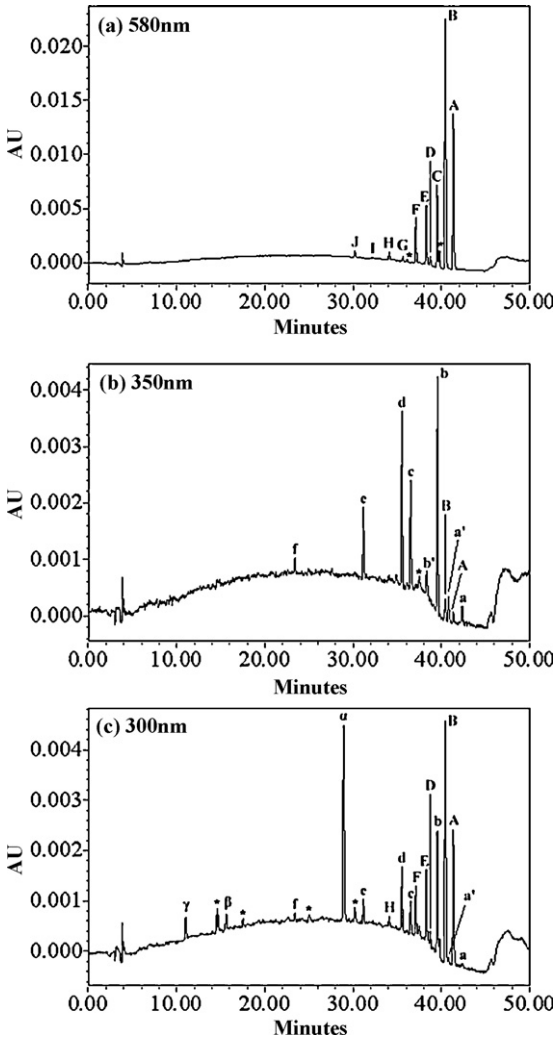

Fig. 9. HPLC chromatogram of intermediates at pH 5 (EV, 10 mg L^{-1}), 36 h of irradiation with UV light, recorded at 580, 350, and 300 nm, imparity was marked with star.

The fourth and fifth groups are marked in the chromatogram and illustrated in Fig. 9c. The *N*-de-ethylation of the DAP, produced by cleavage of the EV chromophore ring structure, has the wavelength position of its major absorption band moved toward the blue region, λ_{max}, α, 302.4 nm; β, 288.1 nm; γ, 284.5 nm. The proposed intermediate (γ) has been compared with standard material of 4-aminobenzophenone. The retention time and absorption spectra are identical.

3.4.2. ESI Mass spectra of the intermediates

The intermediates were further identified using the HPLC-ESI mass spectrometric method, and the relevant mass spectra are illustrated in supporting information (Fig. 2S and Table 2). The molecular ion peaks appeared in the acid forms of the intermediates. The results of mass spectral analysis confirmed that the component A, m/z = 456.57, in liquid chromatogram is EV. The other components are B, m/z = 428.55; C, m/z = 400.42; D, m/z = 400.48; E, m/z = 372.45; F, m/z = 372.52; G, m/z = 344.35; H, m/z = 344.35; I, m/z = 316.32; J, m/z = 288.11; a, m/z = 325.18; b, m/z = 297.46; c, m/z = 269.35; d, m/z = 269.35; e, m/z = 241.20; f, m/z = 213.05; a′, m/z = 341.48; b′, m/z = 313.15.

3.4.3. EI mass spectra of the partial intermediates

The other intermediates were marked in the GC-MS/EI chromatogram, and the relevant mass spectra are illustrated in

Table 2
Intermediates of the photocatalytic degradation of EV identified by HPLC-ESI-MS or GC-EI-MS. Conditions: r24-TiO_2, 10 mg L^{-1} EV, irradiation 36 h.

HPLC peaks	Intermediates	Abbreviation	MS peaks (*m*/*z*)	Absorption maximum (nm)
A	*N*,*N*,*N*′,*N*′,*N*″,*N*″-hexaethylpararosaniline	EV	456.57	590.5
B	*N*,*N*-diethyl-*N*′,*N*′-diethyl-*N*″-ethylpararosaniline	DDEPR	428.55	585.6
C	*N*,*N*-diethyl-*N*′-ethyl-*N*″-ethylpararosaniline	DEEPR	400.42	577.1
D	*N*,*N*-diethyl-*N*′,*N*′-diethylpararosaniline	DDPR	400.48	572.2
E	*N*-ethyl-*N*′-ethyl-*N*″-ethyl pararosaniline	EEEPR	372.45	583.2
F	*N*,*N*-diethyl-*N*′-ethylpararosaniline	DEPR	372.52	574.6
G	*N*-ethy-*N*′-ethylpararosaniline	EEPR	344.35	566.3
H	*N*,*N*-diethylpararosaniline	DPR	344.35	574.9
I	*N*-ethylpararosaniline	EPR	316.32	560.2
J	Pararosaniline	PR	288.11	555.4
a	4-(*N*,*N*-diethylamino)-4′-(*N*′,*N*′-diethylamino)benzophenone	DDBP	325.18	371.6
b	4-(*N*,*N*-diethylamino)-4′-(*N*′-ethylamino)benzophenone	DEBP	297.46	366.7
c	4-(*N*-ethylamino)-4′-(*N*′-ethylamino)benzophenone	EEBP	269.35	362.1
d	4-(*N*,*N*-diethylamino)-4′-aminobenzophenone	DBP	269.35	367.9
e	4-(*N*-ethylamino)-4′-aminobenzophenone	EBP	241.20	357.2
f	4,4′-bis-aminobenzophenone	BP	213.05	340.6
a′	4-(*N*,*N*-diethylamino)-4′-(*N*′-hydroxyethyl-*N*′-ethylamino)benzophenone	DHEBP	341.48	370.4
b′	4-(*N*-hydroxyethyl-*N*-ethylamino)-4′-(*N*′-ethylamino)benzophenone	HEEBP	313.15	367.9
α	4-(*N*,*N*-diethylamino)phenol	DAP	166.27	302.4
β	4-(*N*-ethylamino)phenol	EAP	137.21	288.1
γ	4-Aminophenol	AP	109.19	284.5
I	N,N-diethylaminobenzene	DBz	149	N/A
II	N-ethylaminobenzene	EBz	121	N/A
III	Aminobenzene	ABz	93	N/A
IV	Acetamide	AAm	59	N/A
V	2-Propenoic	PAc	72	N/A
VI	Acetic	AAc	60	N/A

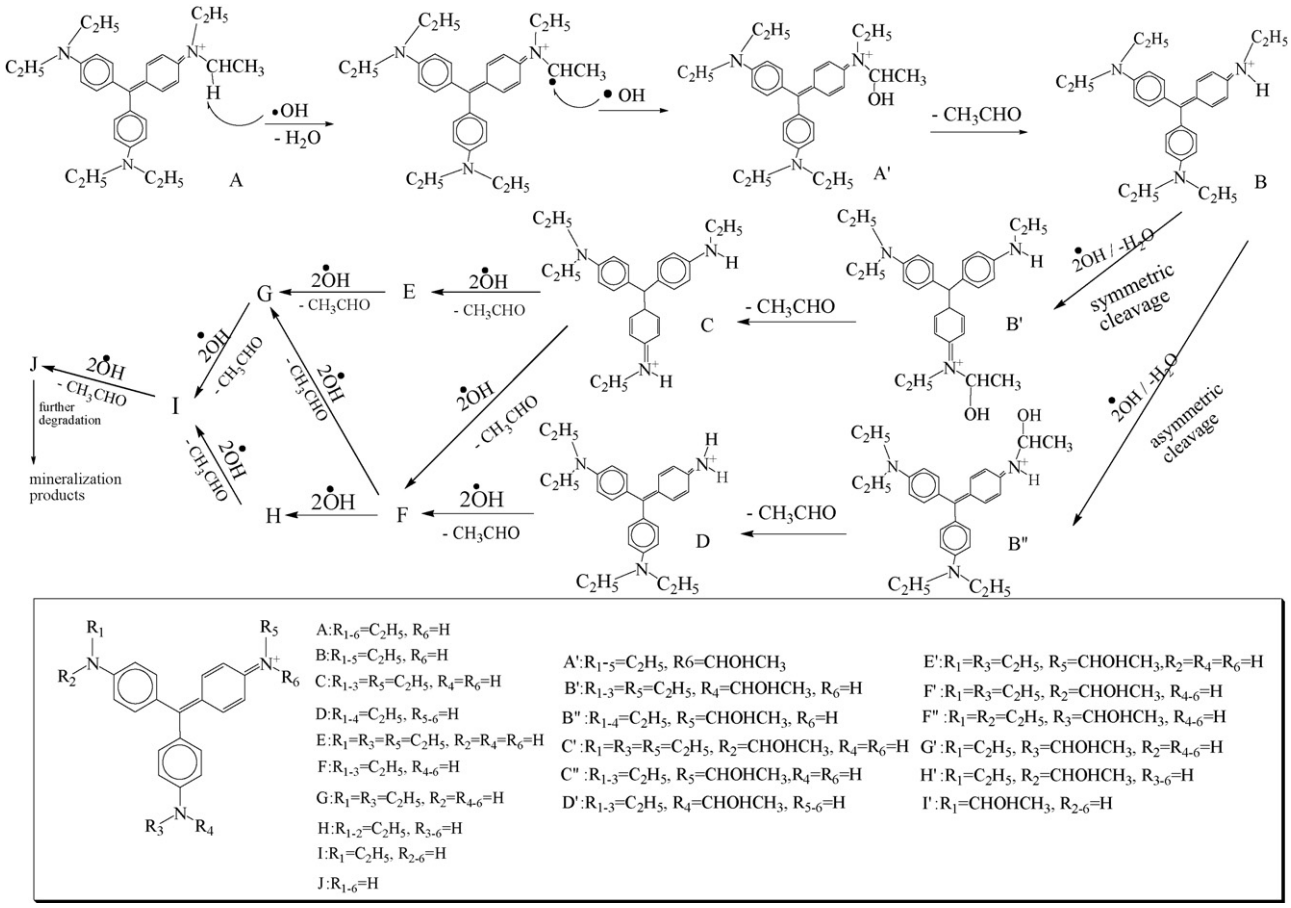

Fig. 10. Proposed *N*-de-ethylation pathway of the EV dye under UV irradiation in aqueous with r24-TiO_2 film followed by the identification of several intermediates by HPLC-ESI mass spectral techniques.

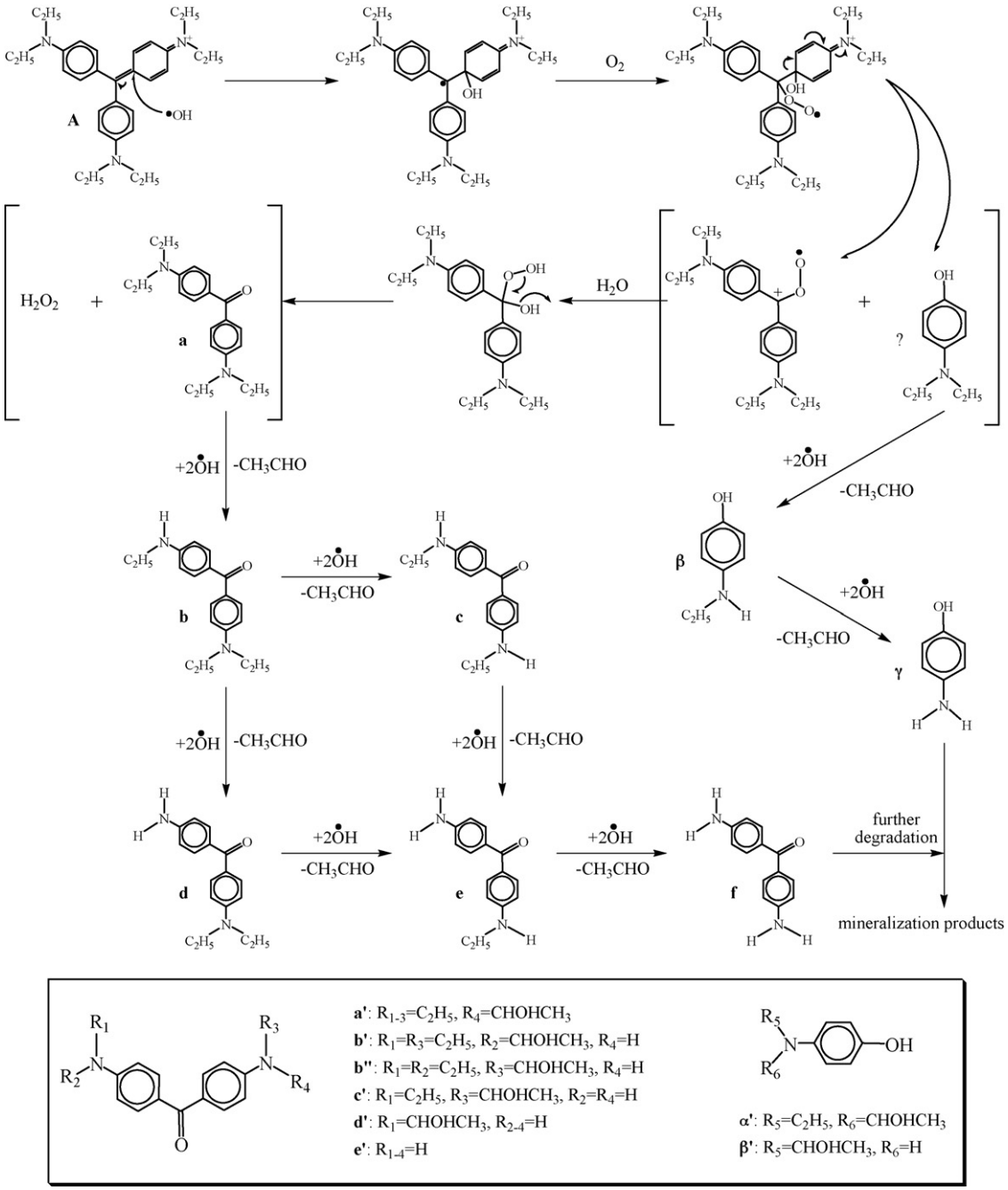

Fig. 11. Proposed pathway of the destruction of the conjugated structure of the EV dye under UV irradiation in aqueous with r24-TiO_2 film followed by the identification of several intermediates by HPLC-ESI mass spectral techniques.

supporting information (Fig. 1S). Table 2 presents the fragmentation patterns of the intermediates (I–VI) and the corresponding compounds identified by interpretation of their MS spectra. The peaks eluting at 30.47, 28.46, 25.58, 23.37, 17.54, and 12.34 min during GC-MS were identified as *N*,*N*-diethylaminobenzene, *N*-ethylaminobenzene, aminobenzene, acetamide, 2-propenoic acid and acetic acid with fit values of 87%, 82%, 83%, 71%, 88%, and 95%, respectively, found by searching the mass spectra library. The intermediates identified in the study were also reported in a previous study of the MEK/TiO_2 system [47]. Further oxidation of organic substrates containing nitrogen to nitrate can be obtained by increasing irradiation time. Results of HPLC chromatograms, UV–vis spectra, HPLC-ESI and GC-EI mass spectra are summarized in Table 2.

3.5. Photodegradation mechanisms of EV

The relative distribution of the intermediates obtained is illustrated in Fig. 3S of supporting information. To minimize errors, the relative intensities were recorded at the maximum absorption wavelength for each intermediate, although a quantitative determination of all of the photogenerated intermediates was not achieved, owing to the lack of appropriate molar extinction coefficients for them and to unavailable reference standards. The distributions of all of the *N*-de-ethylated intermediates are relative to the initial concentration of EV. Nonetheless, we clearly observed the changes in the distribution of each intermediate during the photodegradation of EV. The successive appearance of the maximum of each intermediate indicates that the *N*-de-ethylation of EV, a and α, is a stepwise photochemical process.

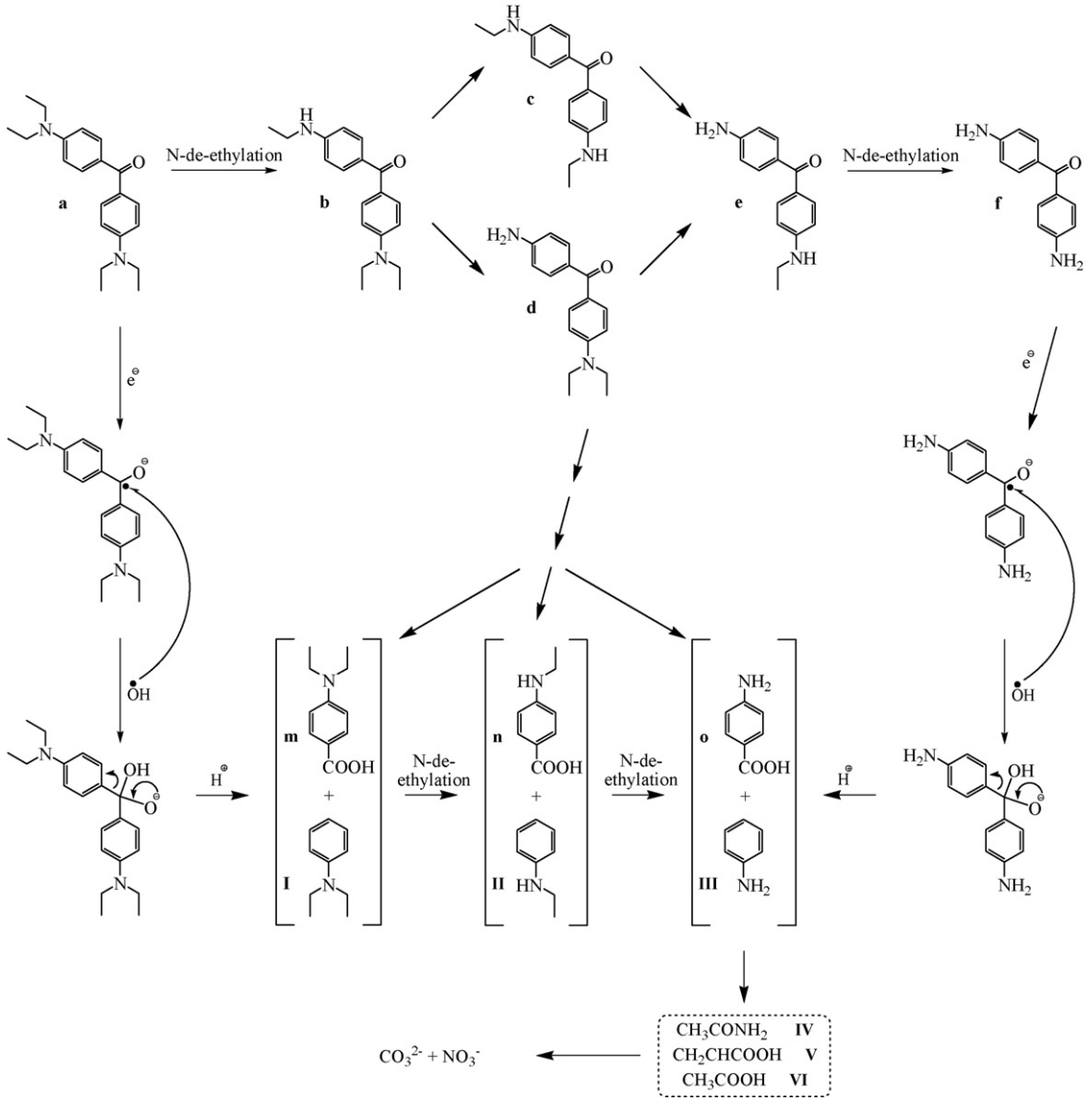

Fig. 12. Proposed pathway of the destruction of the conjugated structure of the 'a' derivatives (compounds I–VI) by the identification of six intermediates by GC-EI mass spectral techniques.

3.5.1. *N*-de-ethylation of EV

Most of the •OH radicals are generated directly from the reaction between the holes and surface-adsorbed H_2O or OH^-. $O_2^{\bullet-}$ should be much less likely to be formed than •OH under UV irradiation [10,43]. The *N*-de-ethylation of the EV dye occurs mostly through attack by the •OH species on the *N*,*N*-diethyl group of EV. The degradation intermediates were clearly observed (Fig. 3S, in supporting information) to reach their maximum concentrations. The concentration of the other intermediates may be too low to be examined by HPLC-PDA-ESI-MS. The results discussed above can be seen more clearly from Fig. 10. EV gets near the negatively charged TiO_2 particle surface via the positive diethylamine group. Then, before the conjugated structure is destroyed, the *N*-de-ethylation occurs preferentially, with the major products being *N*-de-ethylated EV species.

3.5.2. Destruction of the conjugated structure of the EV

The degradation of the EV dye occurs mostly through attack by the •OH species on the central carbon portion of EV and produces a and α. The degradation intermediates were clearly observed (Fig. 3S, in supporting information) to reach their maximum concentrations. The concentration of the other intermediates may be under the detection limit. The results we discussed above can be seen more clearly from Fig. 11. EV is adsorbed on the positively charged TiO_2 particle surface via a conjugated structure. With the major photooxidation products being a, α, their *N*-de-ethylated products, and via *N*-hydroxyethylated intermediates of the de-ethylated products, the cleavage of the EV chromophore structure predominates, and *N*-de-ethylation occurs only to a slight extent.

Further evidence for the pathway(s) of photodegradation was obtained by GC-MS spectroscopic methods. From the results of mass spectral analysis, we identified the major component in the gas chromatograms as *N*,*N*-diethylaminobenzene, *N*-ethylaminobenzene, aminobenzene, acetamide, 2-propenoic acid, and acetic acid. The former intermediates (I–III) detected by GC-MS are the results of the cleavage of intermediates of the third group (a–f), leading to aminobenzene derivatives. The latter intermediates (IV–VI) were formed by cleavage of the aromatic derivatives, leading to aliphatic products. The results we discussed above can be seen more clearly from Fig. 12.

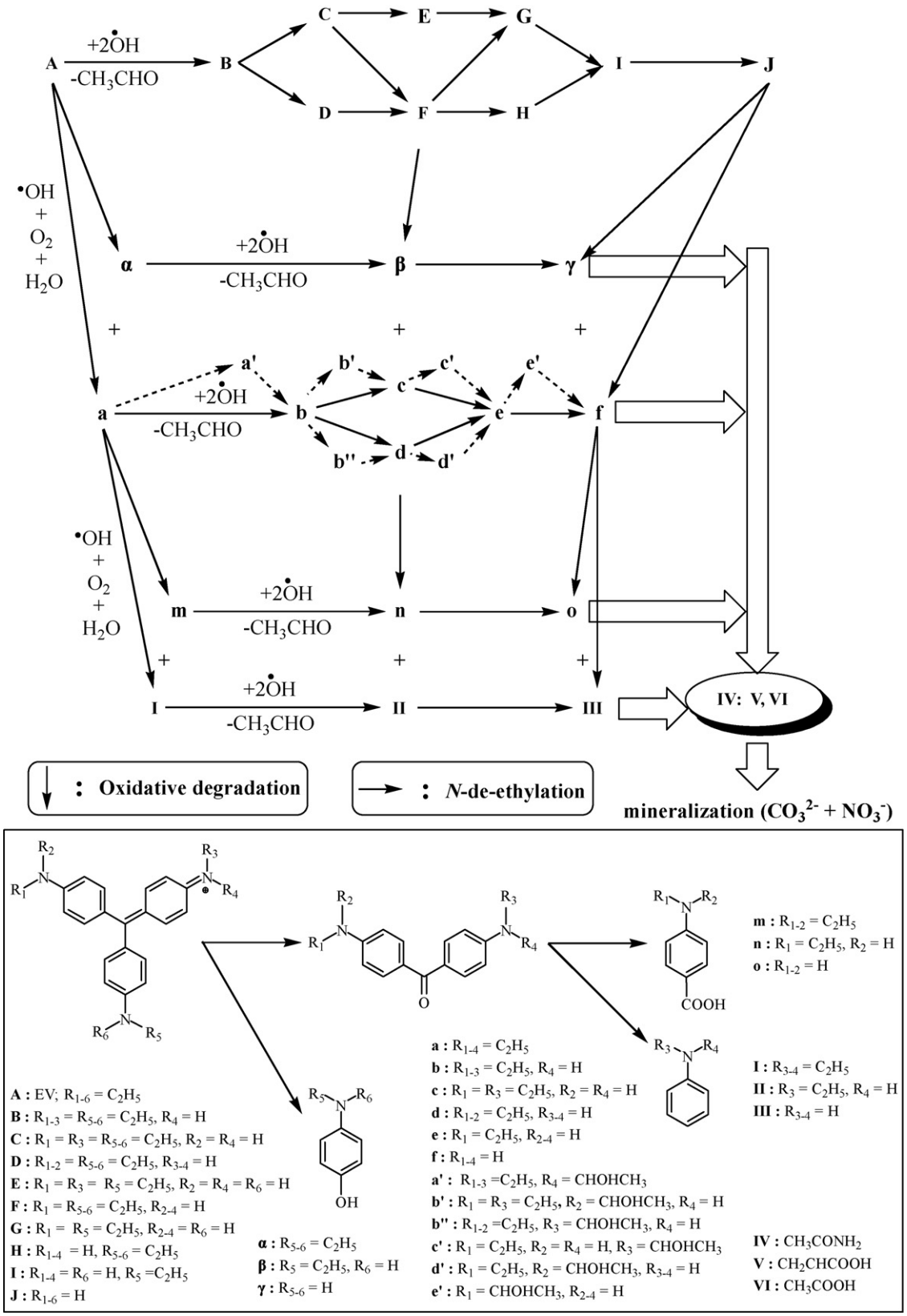

Fig. 13. Proposed pathway of degradated EV dye under UV irradiation in aqueous with r24-TiO_2 film.

3.5.3. The pathways of photocatalytic degradation of the EV

According to earlier reports [13,48–50], most *N*-de-alkylation processes are preceded by the formation of a nitrogen-centered radical while destruction of dye chromophore structures is preceded by the generation of a carbon-centered radical [20,21,25,32,33]. Consistent with this, degradation of EV must occur via two different photodegradation pathways (destruction of the chromophore structure and *N*-de-ethylation) due

to formation of different radicals (either a carbon-centered or nitrogen-centered radical). There is no doubt that the •OH attack on the dye yields a dye cationic radical. After this step, the cationic radical $Dye^{\bullet+}$ can undergo hydrolysis and/or follow various deprotonation pathways, which in turn are determined by the different adsorption modes of EV on the TiO_2 particles surface.

On the basis of all the above experimental results, we tentatively propose the pathway of photodegradation depicted in Fig. 13. In this figure, the dye molecule in the EV/TiO_2 system is adsorbed through the positively charged diethylamine function. Following the attraction by one •OH radical of a hydrogen atom from ethyl group of diethylamine, and the attack by another •OH radical on the diethylamine radical and the formation of hydroxyethylated intermediates, the subsequent hydrolysis (or deprotonation) of intermediates yielded de-hydroxyethylated intermediates, which were subsequently attacked by •OH radicals to lead ultimately to *N*-de-ethylation. The mono-de-ethylated dye derivative, B, can also be adsorbed on the TiO_2 particle surface and is implicated in other similar events (•OH radicals attraction and attack, hydrolysis or deprotonation) to yield the bi-de-ethylated dye derivatives, C and D. The *N*-de-ethylation process as described above continues until formation of the completely de-ethylated dye, J.

In Fig. 13, the dye molecule in the EV/TiO_2 system is adsorbed through a conjugated structure cleavage of the EV chromophore structure. The attack by •OH radical on the conjugated structure yields a carbon-centered radical, which is subsequently attacked by molecular oxygen to lead ultimately to a and α. The same process happened in the *N*-de-ethylated dye to produce the *N*-de-ethylated a and α. The a can also be adsorbed on the TiO_2 particle surface and be implicated in other similar events (•OH radical attraction and attack, hydrolysis or deprotonation, and/or oxygen attack) to yield a mono-*N*-de-ethylated derivative, b. Moreover, the same process happened in α to produce β. The *N*-de-ethylation process as described above continues until formation of the completely *N*-de-ethylated a, f, and *N*-de-ethylated α, γ. All the above *N*-de-ethylation processes produced a series of *N*-de-hydroxyethylated intermediates by the hydroxylation on the *N*-ethyl group. All the intermediates were further degraded to produce *N*,*N*-diethylaminobenzene, *N*-ethylaminobenzene, aminobenzene, acetamide, 2-propenoic acid, and acetic acid, which were subsequently mineralized to lead to CO_3^{2-} and NO_3^- [51].

4. Conclusions

Crystalline porous TiO_2 film has been prepared using hydrothermal treatment of Ti foils in alkali solution. The porous structure of TiO_2 film was analyzed and characterized by XRD, FE-SEM and XPS. Porous TiO_2 film/Ti has demonstrated as a good candidate for dye photocatalytic degradation. In the period of 20 h, the TiO_2 film/Ti as catalyst, both *N*-de-ethylation and conjugated structure of EV dye decomposed, however, the porous TiO_2 film structure remained undisturbed. In addition, the reaction mechanism proposed in this study due to the isolation of stable intermediates. Currently, the porous TiO_2 film/Ti has been modified for the future scale-up applications.

Acknowledgement

This research was supported by the National Science Council of the Republic of China (NSC 97-2113-M-142-002-MY2; NSC 98-2622-M-142-001-CC1).

Appendix A. Supplementary data

Supplementary data associated with this article can be found, in the online version, at doi:10.1016/j.jhazmat.2009.12.113.

References

[1] Ullmann's Encyclopedia of Industrial Chemistry. Part A27. Triarylmethane and Diarylmethane Dyes, sixth ed., Wiley-VCH, New York, 2001.
[2] M.A. Fox, D.F. Duxbury, The photochemistry and photophysics of henylmethane dyes in solid and liquid media, Chem. Rev. 93 (1993) 381–433.
[3] M.R. Hoffman, S.T. Martin, W. Choi, W. Bahnemann, Environmental applications of semiconductor photocatalysis, Chem. Rev. 95 (1995) 69–96.
[4] A.L. Linsebigler, G.Q. Lu, J.T. Yate, Photocatalysis on TiO_2 surfaces: principles, mechanisms, and selected results, Chem. Rev. 95 (1995) 735–758.
[5] C. Nasr, K. Vinodgopal, L. Fisher, S. Hotchandani, A.K. Chattopadhyay, P.V. Kamat, Environmental photochemistry on semiconductor surfaces. Visible light induced degradation of a textile diazo dye, naphthol blue black, on TiO_2 nanoparticles, J. Phys. Chem. 100 (1996) 8436–8442.
[6] C.C. Chen, X. Li, J.C. Zhau, H. Hidaka, N. Serpone, Effect of transition metal ions on the TiO_2-assisted photodegradation of dyes under visible irradiation: a probe for the interfacial electron transfer process and reaction mechanism, J. Phys. Chem. B 106 (2002) 318–324.
[7] W. Chu, C.C. Wong, The hydrogen peroxide-assisted photocatalytic degradation of alachlor in TiO_2 suspensions, Environ. Sci. Technol. 37 (2003) 2310–2316.
[8] J. Lee, W. Choi, J. Yoon, Photocatalytic degradation of N-nitrosodimethylamine: mechanism, product distribution, and TiO_2 surface modification, Environ. Sci. Technol. 39 (2005) 6800–6807.
[9] C.C. Chen, C.S. Lu, Mechanistic studies of the photocatalytic degradation of methyl green: an investigation of products of the decomposition processes, Environ. sci. Technol. 41 (2007) 4389–4396.
[10] T. Wu, G. Liu, J.C. Zhao, H. Hidaka, N. Serpone, Photoassisted degradation of dye pollutants. V. Self-photosensitized oxidative transformation of rhodamine B under visible light irradiation in aqueous TiO_2 dispersions, J. Phys. Chem. B 102 (1998) 5845–5851.
[11] C.C. Chen, H.J. Fan, J.L. Jan, Degradation pathways and efficiencies of acid blue 1 by photocatalytic reaction with ZnO nanopowder, J. Phys. Chem. C 112 (2008) 11962–11972.
[12] G. Liu, X. Li, J.C. Zhao, H. Hidaka, N. Serpone, Photooxidation pathway of sulforhodamine-B. Dependence on the adsorption mode on TiO_2 exposed to visible light radiation, Environ. Sci. Technol. 34 (2000) 3982–3990.
[13] C.C. Chen, C.S. Lu, Photocatalytic degradation of basic violet 4: degradation efficiency, product distribution, and mechanisms, J. Phys. Chem. C 111 (2007) 13922–13932.
[14] B.P. Cho, T. Yang, L.R. Blankenship, J.D. Moody, M. Churchwell, F.A. Bebland, S.J. Culp, Synthesis and characterization of N-demethylated metabolites of malachite green and leucomalachite green, Chem. Res. Toxicol. 16 (2003) 285–294.
[15] G.K.C. Low, S.R. McEvoy, R.W. Matthews, Formation of nitrate and ammonium ions in titanium dioxide mediated photocatalytic degradation of organic compounds containing nitrogen atoms, Environ. Sci. Technol. 25 (1991) 460–467.
[16] K. Nohara, H. Hidaka, E. Pelizzetti, N. Serpone, Processes of formation of NH_4^+ and NO_3^- ions during the photocatalyzed oxidation of N-containing compounds at the titania/water interface, J. Photochem. Photobiol. A: Chem. 102 (1997) 265–272.
[17] S.A. Lee, K.H. Choo, C.H. Lee, H.I. Lee, T. Hyeon, W. Choi, H.H. Kwon, Use of ultrafiltration membranes for the separation of TiO_2 photocatalysts in drinking water treatment, Ind. Eng. Chem. Res. 40 (2001) 1712–1719.
[18] W. Choi, Pure and modified TiO_2 photocatalysts and their environmental applications, Catal. Surv. Asia 10 (2006) 16–28.
[19] J. Ryu, W. Choi, Substrate-specific photocatalytic activities of TiO_2 and multi-activity test for water treatment application, Environ. Sci. Technol. 42 (2008) 294–300.
[20] G.K. Mor, M.A. Carvalho, O.K. Varghese, M.V. Pishko, C.A. Grimes, A room-temperature TiO_2-nanotube hydrogen sensor able to self-clean photoactively from environmental contamination, J. Mater. Res. 19 (2004) 628–634.
[21] Y. Xiong, P.J. Strunk, H. Xia, X. Zhu, H.T. Karlsson, Treatment of dye wastewater containing acid orange II using a cell with three-phase three-dimensional electrode, Water Res. 35 (2001) 4226–4230.
[22] T. Kasuga, M. Hiramatsu, M. Hirano, A. Honson, K. Oyamada, Preparation of TiO_2-based powders with high photocatalytic activities, J. Mater. Res. 12 (1997) 607–609.
[23] I. Saeki, N. Okushi, H. Konno, R. Furuichi, The Photoelectrochemical response of TiO_2–WO_3 mixed oxide films prepared by thermal oxidation of titanium coated with tungsten, J. Electrochem. Soc. 143 (1996) 2226–2230.
[24] B. Karunagaran, R.T.R. Kumar, D. Mangalaraj, S.K. Narayandass, G.M. Rao, Influence of thermal annealing on the composition and structural parameters of DC magnetron sputtered titanium dioxide thin films, Cryst. Res. Technol. 37 (2002) 1285–1292.
[25] M.C. Barnes, S. Kumar, L. Green, N.M. Hwang, A.R. Gerson, The mechanism of low temperature deposition of crystalline anatase by reactive DC magnetron sputtering, Surf. Coat. Technol. 190 (2005) 321–330.
[26] P. Hoyer, H. Masuda, Electrodeposited nanoporous TiO_2 film by a two-step replication process from anodic porous alumina, J. Mater. Sci. Lett. 15 (1996) 1228–1230.

[27] S.Z. Chu, K. Wada, S. Inoue, S.I. Todoroki, Synthesis and characterization of titania nanostructures on glass by Al anodization and sol–gel process, Chem. Mater. 14 (2002) 266–272.
[28] H. Imai, Y. Takei, K. Shimizu, M. Matsuda, H. Hirashima, Direct preparation of anatase TiO_2 nanotubes in porous alumina membranes, J. Mater. Chem. 9 (1999) 2971–2972.
[29] J.M. Macak, M. Zlamal, J. Krysa, P. Schmuki, Self-organized TiO_2 nanotube layers as highly efficient photocatalysts, Small 3 (2007) 300–304.
[30] O.K. Varghese, D. Gong, M. Paulose, C.A. Grimes, E.C. Dickey, Crystallization and high-temperature structural stability of titanium oxide nanotube arrays, J. Mater. Res. 18 (2003) 156–165.
[31] D. Gong, C.A. Grimes, O.K. Varghese, W. Hu, R.S. Singh, Z. Chen, E.C. Dickey, Titanium oxide nanotube arrays prepared by anodic oxidation, J. Mater. Res. 16 (2001) 3331–3334.
[32] V. Zwilling, M. Aucouturier, E. Darque-Ceretti, Electrochim. Acta 45 (1999) 921–929.
[33] E. Balaur, J.M. Macak, H. Tsuchiya, P. Schmuki, Wetting behaviour of layers of TiO_2 nanotubes with different diameters, J. Mater. Chem. 15 (2005) 4488–4491.
[34] S. Funk, B. Hokkanen, U. Burghaus, A. Ghicov, P. Schmuki, Unexpected adsorption of oxygen on TiO_2 nanotube arrays: influence of crystal structure, Nano Lett. 7 (2007) 1091–1094.
[35] C.C. Chen, C.S. Lu, F.D. Mai, C.S. Weng, Photooxidative N-de-ethylation of anionic triarylmethane dye (sulfan blue) in titanium dioxide dispersions under UV irradiation, J. Hazard. Mater. 137 (2006) 1600–1607.
[36] S. Parra, S.E. Stanca, I. Guasaquillo, K.R. Thampi, Photocatalytic degradation of atrazine using suspended and supported TiO_2, Appl. Catal. B: Environ. 51 (2004) 107–116.
[37] J.C. Zhao, H. Hidaka, A. Takamura, E. Pelizzetti, N. Serpone, Photodegradation of surfactants. 11. zeta. Potential measurements in the photocatalytic oxidation of surfactants in aqueous titania dispersions, Langmuir 9 (1993) 1646–1650.
[38] J. Bandara, J.A. Mielczarski, J. Kiwi, 2. photosensitized degradation of azo dyes on Fe, Ti, and Al oxides. Mechanism of charge transfer during the degradation, Langmuir 15 (1999) 7680–7687.
[39] S. Naskar, S. Arumugam, M. Chanda, Photocatalytic degradation of organic dyes in aqueous solution with TiO_2 nanoparticles immobilized on foamed polyethylene sheet, J. Photochem. Photobiol. A: Chem. 113 (1998) 257–264.
[40] L. Lucarelli, V. Nadtochenko, J. Kiwi, Environmental photochemistry: quantitative adsorption and FTIR studies during the TiO_2-photocatalyzed degradation of orange II, Langmuir 16 (2000) 1102–1108.
[41] B. Neppolian, H.C. Choi, S. Sakthivel, B. Arabindoo, V. Murugesan, Solar light induced and TiO_2 assisted degradation of textile dye reactive blue 4, Chemosphere 46 (2002) 1173–1181.
[42] X. Li, G. Liu, J. Zhao, Two competitive primary processes in the photodegradation of cationic triarylmethane dyes under visible irradiation in TiO_2 dispersions, New J. Chem. 23 (1999) 1193–1196.
[43] G. Liu, T. Wu, J. Zhao, H. Hidaka, N. Serpone, Photoassisted degradation of dye pollutants. 8. Irreversible degradation of alizarin red under visible light radiation in air-equilibrated aqueous TiO_2 dispersions, Environ. Sci. Technol. 33 (1999) 2081–2087.
[44] C.C. Chen, C.S. Lu, Y.C. Chung, J.L. Jan, UV light induced photodegradation of malachite green on TiO_2 nanoparticles, J. Hazard. Mater. 141 (2007) 520–528.
[45] L.L. Costa, A.G.S. Prado, TiO_2 nanotubes as recyclable catalyst for efficient photocatalytic degradation of indigo carmine dye, J. Photochem. Photobiol. A: Chem. 201 (2009) 45–49.
[46] A.G.S. Prado, L.L. Costa, Photocatalytic decouloration of malachite green dye by application of TiO_2 nanotubes, J. Hazard. Mater. 169 (2009) 297–301.
[47] C.S. Lu, C.C. Chen, F.D. Mai, Y.C. Wu, Oxidation of styrene by various oxidants with different kinds of metalloporphyrins, J. Photochem. Photobiol. A: Chem. 187 (2007) 167–176.
[48] F.C. Shaefer, W.D. Zimmermann, Dye-sensitized photochemical autoxidation of aliphatic amines in nonaqueous media, J. Org. Chem. 35 (1970) 2165–2185.
[49] B.L. Laube, M.R. Asirvatham, C.K. Mann, Electrochemical oxidation of tropanes, J. Org. Chem. 42 (1977) 670–674.
[50] J.C. Zhao, T. Wu, K. Wu, K. Oikawa, H. Hidaka, N. Serpone, Photoassisted degradation of dye pollutants. 3. Degradation of the cationic dye rhodamine B in aqueous anionic surfactant/TiO_2 dispersions under visible light irradiation: evidence for the need of substrate adsorption on TiO_2 particles, Environ. Sci. Technol. 32 (1998) 2394–2400.
[51] A.B. Prevot, C. Baiocchi, M.C. Brussino, E. Pramauro, P. Savarino, V. Augugliaro, G. Marci, L. Palmisano, Photocatalytic degradation of acid blue 80 in aqueous solutions containing TiO_2 suspensions, Environ. Sci. Technol. 35 (2001) 971–976.